UNIVERSITY OF BRISTOL

Peer reviewed version

Link to published version (if available):
10.1002/anie.201916481

Link to publication record in Explore Bristol Research
PDF-document

University of Bristol - Explore Bristol Research
General rights

Hydrogel-immobilized coacervate droplets as modular micro-reactor assemblies

Jianbo Liu,* [a,b] Liangfei Tian,[b] Yan Qiao,[b] Shaohong Zhou,[a] Avinash J. Patil,[b] Kemin Wang,[a] Mei Li*[b] and Stephen Mann*[b]

Abstract: Immobilization of compartmentalized microscale objects in three-dimensional hydrogels provides a step towards the modular assembly of soft functional materials with tunable architectures and distributed functionalities. Here we use a combination of micro-compartmentalization, immobilization and modularization to fabricate and assemble hydrogel-based micro-reactor assemblies comprising millions of functionalized polysaccharide-polynucleotide coacervate droplets. The heterogeneous hydrogels can be structurally fused by interfacial crosslinking and coupled as input and output modules to implement a UV-induced photocatalytic/ peroxidation nanoparticle/ DNAzyme reaction cascade that generates a spatiotemporal fluorescence read-out depending on the droplet number density, intensity of photo-energization and chemical flux. Our approach offers a route to heterogeneous hydrogels with endogenous reactivity and reconfigurable architecture, and provides a step towards the development of soft modular materials with programmable functionality.

Introduction

Immobilizing micro-compartmentalized synthetic objects such as porous microbeads, liposomes, polymersomes and liquid droplets in three-dimensional (3D) hydrogels offers diverse opportunities for drug delivery and tissue engineering,[1] the assembly of cell-like tissues[2] and organization of spatially distributed microreactors for enhanced mechanical performance, durability and reusability.[3] For example, supramolecular nested microbeads were developed as building blocks to construct macroscopic self-healing scaffolds,[1f] and enzyme-containing hybrid microcapsules hierarchically organized in agarose hydrogels to facilitate recycling of an immobilized biocatalyst.[3b] As individual hydrogels can be shaped and assembled into higher-order arrangements by 3D printing and controlled crosslinking,[1a,4] they provide a potential pathway to the fabrication of soft modular materials based on the integration of

functionally encoded hydrogel building blocks.[1a,5] Such procedures have been primarily exploited for the printing of cell-laden hydrogels from components such as hyaluronic acid[6] and silk fibroin.[7]

Here we describe an approach to the fabrication and assembly of soft matter micro-reactor modules based on the hydrogel-mediated 3D immobilization of dispersed populations of discrete molecularly crowded coacervate micro-droplets[8] containing sequestered photocatalytic nanoparticles, enzymes and DNAzymes. Aqueous suspensions of coacervate droplets have been recently employed as membrane-free micro-reactors capable of *in vitro* gene expression,[9] enhanced protein and RNA catalysis,[10] electric field-induced energization,[11] enzyme-based chemical signaling[12] and artificial predation.[13] Given this wide range of biomimetic activities, we sought to exploit the coacervate droplets as an alternative type of microscale agent for developing multi-functional hydrogel-based modular micro-reactor assemblies. We show that entrapment of the coacervate droplets places diffusional and spatial constraints on their localized reactivity such that fluxes of matter can be established within the hydrogel-based modules. The soft modules can be physically shaped and structurally fused by interfacial crosslinking to produce interconnected multi-functional materials. As proof-of-concept, we prepare a binary arrangement of input and output modules that operate in sequence to implement a UV-energized nanoparticle/DNAzyme photocatalytic/peroxidation cascade reaction under flow conditions. Continuous photo-energization of the input module transmits a hydrogen peroxide (H_2O_2) flux downstream, which in turn activates the spatiotemporal production of a fluorescence readout specifically in the coacervate droplets immobilized along the length of the output module. We show that dynamical changes between the activation and deactivation of fluorescence as the H_2O_2 reaction-diffusion gradient advances along the output module gives rise to a migrating fluorescence band depending on the droplet number density, intensity of the photo-activation and chemical flux originating from the droplet micro-reactors.

Results and Discussion

Preparation of Hydrogel-Based Droplet Micro-Reactor Modules

Hydrogel-based droplet micro-reactor modules were produced by in situ immobilization of millions of intact polysaccharide-polynucleotide coacervate micro-droplets containing sequestered photoactive and catalytic components. Coacervate micro-droplets were pre-prepared at pH 8.0 and room temperature by mixing aqueous solutions of positively charged diethylaminoethyldextran chloride (DEAE-dextran, M_w = 500 kDa) and double-stranded (ds) DNA at a DEAE-dextran : DNA ratio of 2.4 : 1 w/w) (Supporting Information, Figure S1). The

[a]   Dr J. Liu, S. Zhou, Prof. Dr K. Wang
        State Key Laboratory of Chemo/Biosensing and Chemometrics,
        College of Chemistry and Chemical Engineering,
        Key Laboratory for Bio-Nanotechnology and Molecular Engineering
        of Hunan Province,
        Hunan University, Changsha 410082, P. R. China.
        Email: liujianbo@hnu.edu.cn
[b]   Dr J. Liu, Dr L. Tian, Dr Y. Qiao, Dr A. J. Patil, Dr M. Li, Prof. Dr S.
        Mann
        Centre for Protolife Research and Centre for Organized Matter
        Chemistry,
        School of Chemistry, University of Bristol, Bristol BS8 1TS, UK.
        Email: s.mann@bristol.ac.uk, Mei.Li@bristol.ac.uk

        Supporting information for this article is given via a link at the end of
        the document.

molecularly crowded droplets were near-neutral in surface charge (+4.1 mV), polydisperse in size, less than 20 µm in diameter (mean size = 5.3 µm) and exhibited homogeneous green fluorescence after sequestration of the DNA-binding dye SYBR Green (Supporting Information, Figure S2). Capture and immobilization of the DEAE-dextran/dsDNA coacervate droplets at typical loadings of ca. 10^6 droplets per mL was achieved by slowly cooling a hot aqueous agarose solution containing the micro-droplets from 60°C to room temperature (Figures 1a-c). Optical microscopy images showed discrete spherical droplets within the hydrogel that remained unchanged in shape and size for at least 30 days after immobilization (Figure 1d). Increasing the loading to ca. 10^7 droplets mL^{-1} had negligible effect on hydrogel formation and produced a densely crowded 3D distribution of the embedded droplets (Figure 1e). Confocal laser scanning microscopy images indicated that the entrapped droplets were homogeneously distributed throughout the hydrogel matrix (Figure 1f). In contrast, coacervate droplets prepared in the absence of a hydrogel sedimented onto a glass slide within ca. 30 min (Figure 1g). These observations were consistent with SEM images of dried samples, which showed intact or collapsed DEAE-dextran/dsDNA droplets in the presence or absence of an agarose hydrogel, respectively (Supporting Information, Figure S3).

Temperature-dependent rheological measurements showed negligible changes in the solid-like viscoelastic properties of the agarose hydrogels with or without the embedded coacervate micro-droplets. In both cases, thermal hysteresis was observed for the gel-to-sol transition with gelling and melting temperatures of approximately 33.0 ± 1.0 and 90.0 ± 1.0 °C, respectively (Supporting Information, Figure S4). Plots of the shear modulus against strain gave values for the storage (elastic) modulus ($G^{/}$) of ca. 4.3 ×10^3 Pa with $G^{/}$ greater than the loss (viscous) modulus ($G^{//}$) for shear strain values less than 4.0% (Supporting Information, Figure S5).

Hydrogel-based modules comprising immobilized populations of functional coacervate droplets were prepared by partitioning payloads into the molecularly crowded interior of the coacervate micro-droplets prior to hydrogelation. A wide range of functional components were spontaneously sequestered into the DEAE-dextran/dsDNA droplets with high partition coefficients (K). For example: organic dyes (calcein, K = 55; rhodamine 6G, K = 90); enzymes (fluorescein isothiocyanate-labelled glucose oxidase, FITC-GOx, K = 175; horseradish peroxidase, HRP, K = 210); enzyme substrates and products (Amplex red, K = 170; resorufin, K = 160); single-stranded (ss) oligonucleotides (cyanine-5 (Cy5)-ssDNA, K = 560), a G-quadruplex (G4-hemin DNAzyme, K = 145); and inorganic nanoparticles (N-acetylcysteine-capped cadmium telluride quantum dots, NAC-CdTe, K = 340; photocatalytic TiO_2/Ag hybrid clusters, K = 770). In each case, the functional payloads were spatially localized at the micrometre scale within the agarose matrix by compartmentalization within the entrapped DEAE-dextran/dsDNA droplets (Figures 2a-f and Supporting Information, Figure S6). Subjecting the hydrogel modules to gel electrophoresis showed minimal movement of the guest components out of the agarose matrix (Supporting Information, Figure S7), consistent with their high binding affinity to the coacervate phase.

Functional Modules and Modular Assembly

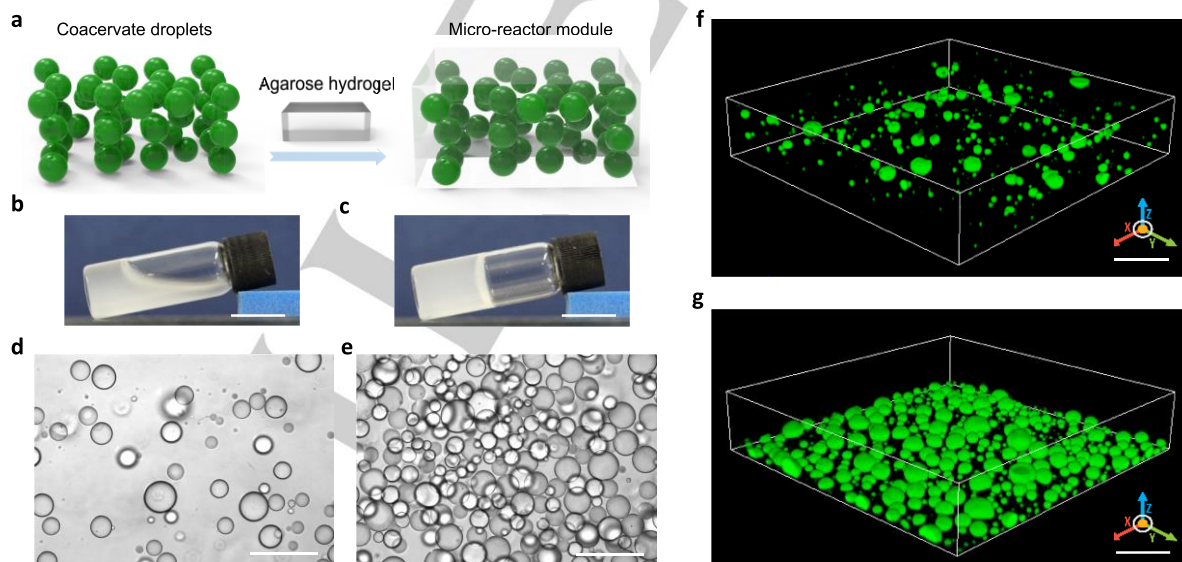We exploited the high loading capacity of the DEAE-dextran/dsDNA coacervate droplets to prepare a single

Figure 1. Preparation of a hydrogel-based droplet micro-reactor module. a) Scheme illustrating capture and immobilization of DEAE-dextran/*ds*DNA coacervate micro-droplets in an idealized agarose hydrogel to produce a hydrogel-based droplet micro-reactor module. b,c) Photographs of a coacervate micro-droplet aqueous suspension (DEAE-dextran (12.0 mg mL^{-1})/*ds*DNA (5.0 mg mL^{-1})) before (b) and after *in situ* hydrogelation (c). Hydrogelation was initiated by addition of an equal volume of 1 wt% agarose at 60°C followed by cooling to room temperature; scale bars: 20 mm. d,e) Optical microscopy images of micro-reactor modules comprising *ca.* 10^6 (d) or 10^7 coacervate droplets mL^{-1} (e) embedded within an agarose hydrogel (0.5 wt%) after storage for 30 days at room temperature; scale bars; 10 µm. f,g) Confocal fluorescence microscopy images of a population of DEAE-dextran/DNA coacervate droplets showing a homogeneous 3D distribution when immobilized within the agarose hydrogel (f); in contrast, the droplets sediment onto a glass slide in the absence of a hydrogel (g). Coacervate droplets were stained with the DNA binding dye SYBR-green; scale bars: 20 µm.

hydrogel-based droplet micro-reactor module capable of processing a localized two-step enzyme cascade. For this, we co-sequestered GOx, HRP and Amplex red in the droplets, embedded the loaded droplets within the hydrogel, and then added glucose to trigger GOx-mediated formation of hydrogen peroxide (H_2O_2). Subsequent H_2O_2/HRP-mediated peroxidation of Amplex red to resorufin was confirmed by fluorescence microscopy images, which showed red fluorescence predominantly within the immobilized coacervate micro-droplets (Figure 2g). The kinetic profiles were fitted to a Michaelis–Menten model with values for the Michaelis constant (K_m) and turnover number (k_{cat}) of 120 mM, and 120 s^{-1}, respectively (Figure 2h and Supporting Information, Figure S8). These values were different from those determined in an agarose hydrogel matrix prepared in the absence of the coacervate droplets (K_m, 82 mM; K_{cat}, 190 s^{-1}), suggesting that the glucose binding efficiency was reduced in the modules, possibly due to partial deactivation of the enzymes in the presence of high polyelectrolyte concentrations. However, direct comparison of the kinetic profiles was ambiguous given that the effective concentrations of enzymes and substrates partitioned within the coacervate droplets were higher than those in the bulk phase, and that diffusional limitations due to rapid substrate depletion in the coacervate droplets could not be ruled out. Nevertheless, it

seemed clear that the large loading capacity of the coacervate microdroplets for GOx and HRP (K = 175 and 210, respectively) gave rise to enhanced levels of enzyme activity in the micro-reactor module compared with hydrogels loaded with the same enzyme concentrations but prepared in the absence of coacervate micro-droplets (Supporting Information, Figure S9).

Given the above observations, we constructed self-supporting stacks of DEAE-dextran/dsDNA hydrogels comprising multiple zones of matrix-immobilized coacervate-based droplet micro-reactors. For this, alginate (1 wt%; agarose/alginate volume ratio = 1 : 1), was added to the agarose hydrogels to enable sequential adhesion of individual reaction modules via Ca^{2+}-induced crosslinking (Supporting Information, Figure S10). Three separate agarose/alginate hydrogels containing embedded coacervate micro-droplets loaded with FITC-GOx, NAC-CdTe or Cy5-DNA were prepared individually in 16 mm-diameter glass tubes comprising a detachable stopper. Each material was gently removed using a glass rod and the modules attached at their ends in a stepwise fashion by immersion in aqueous 50 mM $CaCl_2$ solution for 4 h at room temperature. The resulting cylindrical stack comprised discrete zones of green, yellow and red fluorescence that were joined
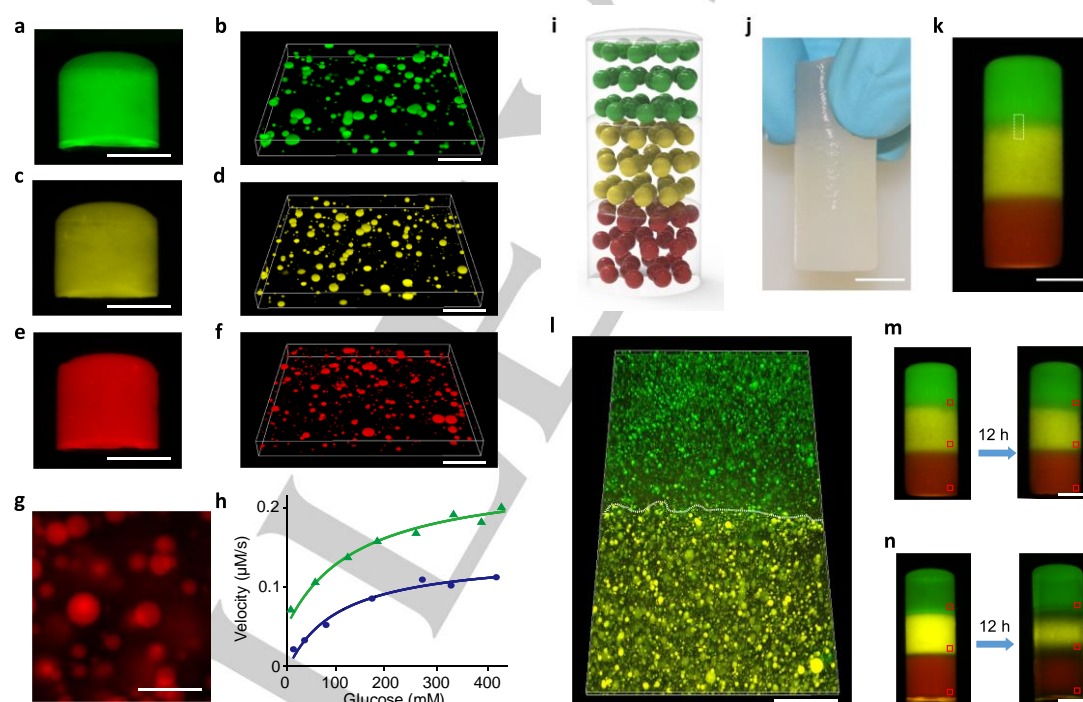

Figure 2. Functional modules and modular assembly. a,b) Fluorescence microscopy images of a bulk hydrogel containing an entrapped population of FITC-GOx-loaded DEAE-dextran/*ds*DNA coacervate droplets ((a), module **1**), and corresponding confocal image of the homogeneous 3D distribution of immobilized droplets (b) (green fluorescence, FITC-GOx; 10^6 droplets mL^{-1}); scale bars = 10 mm (a) and 20 μm (b). c-f) As for (a) and (b) but for hydrogel-based modules **2** (c,d) and **3** (e,f) functionalized with NAC-CdTe quantum dots (yellow fluorescence) or Cy5-DNA (red fluorescence), respectively; scale bars, 10 mm (c,e) and 20 μm (d,f). g) Fluorescence microscopy image showing red fluorescence associated with resorufin production specifically within hydrogel-immobilized coacervate droplets containing GOx, HRP and Amplex red after addition of glucose (10 mM); scale bar, 20 μm. h) Plots of initial rate of enzyme activity against glucose concentration for GOx/HRP cascade reactions in a hydrogel matrix (0.5% wt agarose, pH = 7.4, green triangles) or within hydrogel-immobilized coacervate droplets (0.5% wt agarose, *ca*. 10^6 coacervate droplets mL^{-1}, pH=7.4, blue circles). (GOx, 33 mU mL^{-1} (added concentration, C_o) = 486 mU mL^{-1} (sequestered concentration, C_s); HRP, 1 U mL^{-1} (C_o) and 15 U mL^{-1} (C_s); Amplex red, 16.7 μM (C_o) and 250 μM (C_s). i-k) Three-level stack prepared from sequential Ca^{2+}-mediated crosslinking of modules **1**, **2** and **3**; graphic shows the idealized 3D arrangement of the stack (i), and optical and fluorescence microscopy images are shown in (j) and (k), respectively; scale bars, 10 mm. l) Scanning confocal fluorescence microscopy image of the adhesion interface (dotted white line) between modules **1** and **2**. The imaged area is denoted by the small rectangular white box shown in (k); scale bar: 100 μm. m) Fluorescence microscopy images recorded 12 h after immersion of a linear stack of modules **1**, **2** and **3** in water in the dark showing no changes in fluorescence intensities; scale bar, 10 mm. n) As for (m) but in the absence of entrapped coacervate droplets showing *ca.* 37% decrease in fluorescence intensity at the boundaries of the modules due to inter-zonal diffusion; scale bar, 10 mm.

continuously across their interfaces (Figures 2i-k). Scanning confocal fluorescence microscopy images of the adhesion interfaces showed a clear demarcation in the positioning of the sequestered FITC-GOx, NAC-CdTe or Cy5-DNA components (Figure 2l). Moreover, time-lapse images recorded over a period of 12 h showed no significant changes in the fluorescence intensities associated with the different modules, indicating that the constituent coacervate micro-droplets and their functional components remained immobilized within the stacked hydrogel matrix (Figure 2m and Figure S11). In contrast, FITC-GOx, NAC-CdTe and Cy5-DNA migrated across the hydrogel boundaries in the absence of the entrapped coacervate micro-droplets (Figure 2n). We attribute these differences to the high sequestration potential of the molecularly crowded DEAE-dextran/dsDNA droplets. This was consistent with a series of experiments that showed that release of the guest molecules from the coacervate-containing hydrogel matrix into the bulk aqueous phase was strongly inhibited when compared with leaching rates measured for coacervate-free hydrogels (Supporting Information, Figure S12).

Photocatalytic/Peroxidation Serial Processing Under Flow Conditions

Given that individual hydrogel-based droplet micro-reactor modules could be structurally integrated by interfacial crosslinking, we prepared a construct comprising a binary combination of modules capable of serial processing a UV-initiated nanoparticle/DNAzyme photocatalytic/peroxidation cascade reaction under flow conditions (Figures 3a,b). The upstream input module consisted of a population of hydrogel-immobilized DEAE-dextran/dsDNA coacervate droplets containing high concentrations of sequestered positively charged TiO_2/Ag nanoparticles (K = 770) capable of UV-light induced reduction of dioxygen to H_2O_2 (Supporting Information, Figures S13 and S14).[14] We tested the viability of the input module by determining the yield of H_2O_2 produced by photo-excitation under UV irradiation (365 nm, 60 min) using an ABTS colorimetric assay in the absence of any auxiliary electron donor. We compared the results with yields obtained under the same conditions but from aqueous dispersions of TiO_2/Ag nanoparticle-containing coacervate droplets or TiO_2/Ag nanoparticles alone (Figure 3c); in both cases, significant and similar yields of H_2O_2 were observed (38 and 30 μM, respectively), indicating that sequestration of the nanoparticles within the coacervate droplets did not deactivate the photocatalytic components. Embedding the TiO_2/Ag-loaded coacervate droplets in an agarose/alginate hydrogel slightly reduced the photocatalytic yield to a value of 28 μM, possibly due to scattering of the UV light by the hydrogel matrix.

The downstream output module comprised a similar arrangement of hydrogel-immobilized coacervate droplets as present in the input module but in place of the inorganic nanoparticles the micro-droplets were loaded with Amplex red (K = 170) and a single-stranded G4-hemin DNAzyme (K = 145) capable of functioning as a peroxidase-mimic in the presence of H_2O_2.[15] As a consequence, addition of H_2O_2 to the module gave rise to red fluorescence (resorufin production) specifically within the embedded DEAE-dextran/dsDNA coacervate droplets (Figure 3d), indicating that the G4-hemin DNAzyme remained active after sequestration and immobilization. Time-dependent changes in the fluorescence intensity recorded at 585 nm

indicated that the DNAzyme activity was reduced within the coacervate micro-droplets whether in suspension (initial rate, 60 nM s^{-1}) or immobilized within the hydrogel (11 nM s^{-1}) compared with the value determined in free solution (130 nM s^{-1}) (Figure 3e).

Having established that the individual hydrogel-based droplet micro-reactor modules were functionally active, we prepared input and output modules with disk-like and rectangular morphologies, respectively, and connected them in series by interfacial crosslinking. In so doing, we produced an arrangement capable of implementing a photocatalytic/peroxidation cascade under reaction-diffusion conditions (Supporting Information, Figure S15). Continuous exposure of the upstream input module to UV irradiation resulted in TiO_2/Ag nanoparticle-mediated photocatalytic reduction of dioxygen within the embedded coacervate droplets followed by mass transport of H_2O_2 into the output module. Subsequent oxidation of Amplex red to resorufin by G4-hemin-mediated peroxidation within the immobilized coacervate droplets gave rise to a red fluorescence output specifically in the output module. Moreover, because the resorufin fluorescence was quenched at high concentrations of H_2O_2 by molecular degradation to resazurin,[16] the high H_2O_2 diffusion gradient generated in the input module produced a fluorescent band that migrated along the reaction-diffusion field in the output domain (Figure 3f). This effect was attributed to dynamical changes between the activation and deactivation of fluorescence as the H_2O_2 chemical gradient advanced along the output module during which resorufin was produced by G4-hemin activity and then degraded in situ as the H_2O_2 concentration reached a critical value (typically above 500 μM; Supporting Information, Figure S16).

We tested the coupling of the photocatalytic input and peroxidase output modules under different conditions. In general, optical and fluorescence monitoring of the interface between the two micro-reactor modules showed a clear demarcation in the formation of resorufin specifically at the output side of the boundary (Supporting Information, Figure S17). Continuous exposure of the input module to UV-light produced a diffusive downstream flow of H_2O_2 such that a time-dependent red fluorescence readout migrated progressively along the length of the output module. For example, under close to optimum conditions (10^6 droplets mL^{-1}; input module, 50 mW UV, TiO_2/Ag = 1 mg mL^{-1}; output module, G4-hemin = 0.5 μM, Amplex red = 25 μM), the fluorescence intensity, which attained a steady state value after 15 min, migrated along the output module at a linear rate of ca. 2.0 μm s^{-1} (Figure 3f and Movie S1). Significantly, as shown in Figure 3f, the tail of the fluorescence output was progressively quenched with time such that the readout became spatiotemporally organized to produce a moving front that increased marginally in width along the chemical gradient (Figure 3g). High resolution fluorescence profiles recorded at different positions along the length of the output module indicated that the fluorescence was activated locally after a specific delay time, increased in intensity to a maximum value as the localized Amplex red was consumed and resorufin produced, and then decayed at a relatively slower rate over a period of 100-150 min as the H_2O_2 increased in concentration (Figure 3h). As a consequence, the width of the migrating fluorescence band remained essentially constant when the rates of fluorescence activation and deactivation were approximately equal at the front

and tail of the band, respectively. In practice, both processes were accompanied by peak broadening as the band moved along the output module due to shear-induced dispersion of the chemical gradient (Supporting Information, Figure S18).

We used a fluorescence recovery after photobleaching (FRAP) experiment to confirm that diffusion of the resorufin signal along the output module was severely restricted in the presence of the coacervate micro-droplets (Supporting Information, Figure S19). No fluorescence recovery was observed over a period of 250 s in the presence of the immobilized coacervate droplets, consistent with strong partitioning of the fluorescence read-out specifically within the droplet micro-reactors. In contrast, ca. 77% of the red

fluorescence intensity was recovered in this time period for resorufin-containing coacervate-free hydrogels. As a consequence, UV-energization of an identical system fabricated in the absence of the coacervate droplets produced a continuous red fluorescence band along the entire output module due to unrestricted diffusive mixing of Amplex red and resorufin (Supporting Information, Figure S20). Similar observations were recorded when the number of hydrogel-immobilized droplets was reduced from 10^6 to 10^5 droplets mL^{-1} (Supporting Information, Figure S21), indicating that emergence of the migrating resorufin front was dependent on a critical number density of embedded micro-reactor droplets.
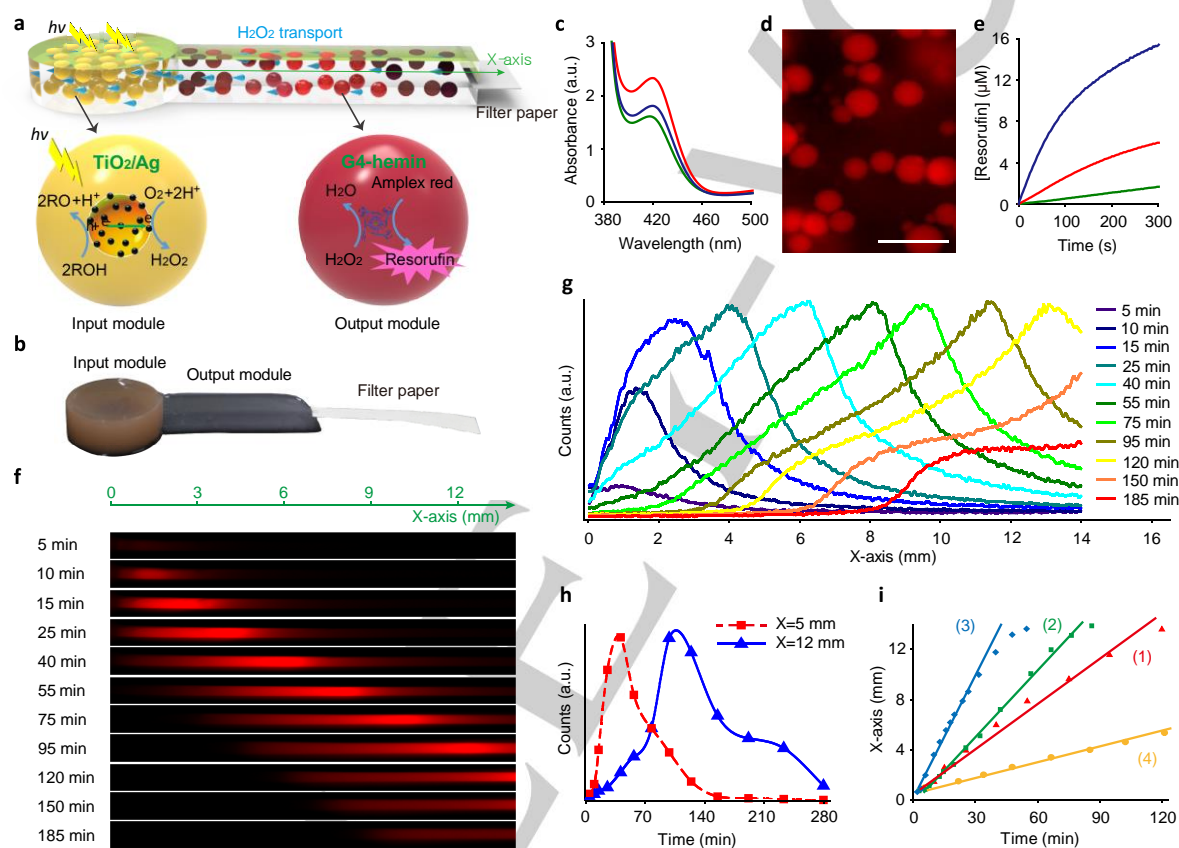

Figure 3. Photocatalytic/peroxidation serial processing under flow conditions. a) Graphical representations: linear arrangement of two hydrogel-based droplet micro-reactor modules operating collectively as a photocatalytic/peroxidation cascade (top) under flow conditions, and details of the upstream input (TiO$_2$/Ag nanoparticles, yellow image, bottom left) and downstream output (G4-hemin DNAzyme, red image, bottom right) modules. Exposure of the input module to UV irradiation results in H$_2$O$_2$ production followed by downstream diffusive flow into the output module and subsequent formation of a red fluorescence readout (resorufin). Unidirectional liquid flow along the *x* axis is facilitated by attaching a strip of filter paper downstream of the output module and by gradual addition of water in front of the input zone. b) Photograph showing experimental set-up. Typically, the input and output modules were 16 mm and 20 mm in diameter and length, respectively. c) UV-vis absorption spectra showing bands at 420 nm corresponding to the formation of oxidized [ABTS$^{\cdot-}$] due to photocatalytic H$_2$O$_2$ production in the presence of TiO$_2$/Ag nanoparticles dispersed in bulk solution (blue), or sequestered within coacervate droplets dispersed in aqueous solution (red), or immobilized within an agarose/alginate hydrogel (input module, green); a.u = arbitrary units. d) Fluorescence microscopy image (excitation, 561 nm; emission, 585 nm) of the output module after addition of aqueous H$_2$O$_2$ (10 μL, 10 mM) showing red fluorescence resorufin) in the coacervate droplets; scale bar, 20 μm. e) Time-dependent plots showing increases in resorufin concentration associated with DNAzyme activity in aqueous solution (blue), sequestered within coacervate droplets dispersed in aqueous solution (red), or immobilized within an agarose/alginate hydrogel (output module, green). f) Time-lapse fluorescence microscopy images recorded from the output module showing the downstream propagation of a resorufin red fluorescence band (*x* axis; *x* = 0 at input/output interface). Experimental conditions: 10^6 droplets mL^{-1}; input module (not imaged), 50 mW UV (continuous), TiO$_2$/Ag = 1 mg mL^{-1} (added concentration, C_o) = 15.7 mg mL^{-1} (sequestered concentration, C_s); output module, G4-hemin = 0.5 μM (C_o) and 7.3 μM (C_s), Amplex red = 25 μM (C_o) and 368 μM (C_s). g) Plots of red fluorescence intensity along the output module (*x* axis) as shown in (f) recorded at various time intervals over a period of 185 min. h) Corresponding time-dependent changes in red fluorescence at *x* = 5 mm (red) and *x* = 12 mm (blue) showing fluorescence activation and quenching. A period of *ca.* 55 min separates the two resorufin readouts. i) Plots of fluorescence peak positions with time for resorufin bands produced under different reaction conditions. All experiments performed with continuous UV irradiation, 10^6 droplets mL^{-1}, TiO$_2$/Ag = 1 mg mL^{-1} (C_o) and 15.7 mg mL^{-1} C_s) and G4-hemin = 0.5 μM (C_o) and 7.3 μM (C_s) with the following specifications: **1** (red triangles), 50 mW UV, Amplex red = 25 μM (C_o) and 368 μM (C_s); **2** (green squares), 100 mW UV, Amplex red = 25 μM (C_o) and 368 μM (C_s); **3** (blue diamonds), 50 mW UV, Amplex red = 8 μM (C_o) and 118 μM (C_s); **4** (yellow circles), 50 mW UV, Amplex red = 25 μM (C_o) and 368 μM (C_s), catalase = 10 pM (C_o) and 147 pM (C_s). Constant migration speeds of 2.0, 2.9, 4.2 and 0.7 μm s^{-1} were observed, respectively, along the *x* axis.

Other experiments indicated that the reaction-diffusion process was also influenced by time-dependent changes in the localized H_2O_2, Amplex red and resorufin concentrations. As such, coupling between the input and output modules could be modified by altering the fluxes used to establish the photocatalytic/peroxidase cascade. For example, increasing the power of the continuous UV-light source from 50 to 100 mW increased the migration rate of the fluorescence band from 2.0 to ca. 2.9 µm s^{-1} due to the increase in the H_2O_2 concentration gradient generated in the input module (Supporting Information, Figure S22). The rate of propagation was increased to ca. 4.2 µm s^{-1} when the concentration of sequestered Amplex red was decreased to 8 µM (Supporting Information, Figure S23). We attributed this to an increase in the H_2O_2 flux associated with the reduced levels of H_2O_2 depletion from the advancing concentration gradient at higher $[H_2O_2]/[Amplex red]$ and $[H_2O_2]/[resorufin]$ molar ratios. In contrast, a decrease in the speed of the fluorescence band to ca. 0.7 µm s^{-1} was obtained by co-sequestration of catalase into the coacervate droplets contained within the output module (Supporting Information, Figure S24). Under these conditions, catalase activity in the droplets provided a competitive enzyme-mediated pathway for consumption of the H_2O_2 as it diffused along the chemical gradient.

A simplified model of the spatiotemporal distribution of resorufin along the output module was developed to simulate the emergence and propagation of the fluorescent band. Using a finite explicit approach with closed boundary conditions we calculated the mass balance at different locations of the unidirectional H_2O_2 chemical gradient assuming that the production and depletion of resorufin occurred in two discrete steps and that H_2O_2 in the input module was photocatalytically generated at a continuous rate of 0.1 µM s^{-1} (Supporting Information, Figure S25). The calculated 1D time-dependent distributions of resorufin in the simulated hydrogel-based reactor migrated progressively along the length of the output module, consistent with the experimental observations and in agreement with a dynamical process involving both fluorescence activation and deactivation.

Conclusion

In conclusion, we describe an approach to the fabrication and assembly of micro-reactor modules based on the hydrogel-mediated immobilization of dispersed suspensions of molecularly crowded DEAE-dextran/dsDNA coacervate micro-droplets containing photocatalytic nanoparticles, enzymes and DNAzymes. The ability of coacervates to sequester high concentrations of guest components compared with conventional water-containing droplets prepared by emulsification or vesicularization for example offers a straightforward approach to droplet-based micro-reactors with high cargo loading. Moreover, entrapment of high number densities of the reactive coacervate droplets in agarose/alginate polysaccharide hydrogels provides a facile approach to developing spatially segregated populations of micro-reactors that can be assembled into input and output modules by interfacial crosslinking. Immobilization of the droplets imposes spatial and diffusional barriers on their localized reactivity such

that the hydrogel-based modules can be internally connected by the flow of molecular intermediates and selectively interfaced with the surrounding environment using UV-irradiation. As a consequence, we demonstrate a UV-induced photocatalytic/peroxidation nanoparticle/DNAzyme cascade with a spatiotemporal fluorescence read-out specifically along the output module, which depends on the droplet number densities, intensity of photo-energization in the input module and the downstream flux of H_2O_2. These factors influence the dynamical changes between the activation and deactivation of fluorescence as the H_2O_2 reaction-diffusion gradient advances along the output module to produce a read-out in the form of a migrating fluorescence band. The system operates efficiently due to the relatively high diffusion coefficient of H_2O_2 but is likely to become less effective when the carrier is a larger molecule. Taken together, our work offers a promising approach to heterogeneous hydrogels with endogenous reactivity, reconfigurable architecture and programmable functionality for potential uses in areas such as bioengineering and flow chemistry.

[1] a) M.Y. Chiang, Y.W. Hsu, H.Y. Hsieh, S.Y. Chen, S.K. Fan, *Sci. Adv.* **2016**, *2*, e1600964; b) F. Pati, J. Jang, D.H. Ha, S. Won Kim, J.W. Rhie, J.H. Shim, D.H. Kim, D.W. Cho, *Nat Commun.* **2014**, *5*, 3935; c) J. L. Guo, Y. S. Kim, V. Y. Xie, B. T. Smith, E. Watson, J. Lam, H. A. Pearce, P. S. Engel, A. G. Mikos, *Sci. Adv.* **2019**, *5*, eaaw7396; d) M. Marguet, C. Bonduelle, S. Lecommandoux, *Chem. Soc. Rev.* **2013**, *42*, 512-529; e) I. Kusters, N. Mukherjee, M.R. de Jong, S. Tans, A. Koçer, A.J.M. Driessen, *PLOS One* **2011**, *6*, e20435; f) Z. Yu, J. Liu, C.S.Y. Tan, O.A. Scherman, C. Abell, *Angew. Chem. Int. Ed.* **2018**, *57*, 3079-3083.

[2] a) D. K. Baxani, A. J. L. Morgan, W. D. Jamieson, C. J. Allender, D. A. Barrow, O. K. Castell, *Angew. Chem. Int. Ed.* **2016**, *55*, 14240-14245; b) M. Mariam Bayoumi, H. Bayley, G. Maglia, K. T. Sapra, *Sci. Rep.* **2017**, *7*, 45167.

[3] a) H.P. De Hoog, I.W. Arends, A.E. Rowan, J.J. Cornelissen, R.J. Nolte, *Nanoscale* **2010**, *2*, 709–716; b) S. Zhang, Z. Jiang, J. Shi, X. Wang, P. Han, W. Qian, *ACS Appl. Mater. Interfaces* **2016**, *8*, 25152–25161.

[4] O.F. Khan, D.N. Voice, B.M. Leung, M.V. Sefton, *Adv. Healthcare Mater.* **2015**, *4*, 113–120.

[5] A. Nadernezhad, N. Khani, G.A. Skvortsov, B. Toprakhisar, E. Bakirci, Y. Menceloglu, S. Unal, B. Koc, *Sci. Rep.* **2016**, *6*, 33178.

[6] K.M. Park, J.A. Yang, H. Jung, J. Yeom, J.S. Park, K.H. Park, A.S. Hoffman, S.K. Hahn, K. Kim, *ACS Nano* **2012**, *6*, 2960-2968.

[7] S.H. Kim, Y.K. Yeon, J.M. Lee, J.R. Chao, Y.J. Lee, Y.B. Seo, M.T. Sultan, O.J. Lee, J.S. Lee, S.I. Yoon, I.S. Hong, G. Khang, S.J. Lee, J.J. Yoo, C.H. Park, *Nat Commun.* **2018**, *9*, 1620.

[8] a) S. Koga, D. S. Williams, A. W. Perriman, S. Mann, *Nat. Chem.* **2011**, *3*, 720-724; b) W. M. Aumiller, C. D. Keating, *Nat. Chem.* **2016**, *8*, 129-

137; c) K. K. Nakashima, J. F. Baaij, E. Spruijt, *Soft Matter* **2018**, *14*, 361-367.

[9]   D. T.-Y. Tang, D. van Swaay, A. deMello, J. L. Ross Anderson, S. Mann, *Chem. Commun.* **2015**, *51*, 11429-11432.

[10]   a) J. Crosby, T. Treadwell, M. Hammerton, K. Vasilakis, M. P. Crump, D. S. Williams, S. Mann, *Chem. Commun.* **2012**, *48*, 11832-11834; b) B. Drobot, J. M. Inglesias-Artola, K. Le Vay, V. Mayr, M. Kar, M. Kreysing, H. Mutschler, T.-Y. D. Tang, *Nat. Commun.* **2018**, *9*, 3643; c) R. R. Poudyal, R. M. Guth-Metzler, A. J. Veenis, E. A. Frankel, C. D Keating, P. C. Bevilacqua, *Nat. Commun.* **2019**, *10*, 490.

[11]   Y. Yin, L. Niu, X. Zhu, M. Zhao, Z. Zhang, S. Mann, D. Liang, *Nat. Commun.* **2016**, *7*, 10658.

[12]   L. Tian, N. Martin, P. G. Bassindale, A. J. Patil, M. Li, A. Barnes, B. W. Drinkwater, S. Mann, *Nat. Commun.* **2016**, *7*, 13068.

[13]   Y. Qiao, M. Li, R. Booth, S. Mann, *Nat. Chem.* **2017**, *9*, 110-119.

[14]   D. Tsukamoto, A. Shiro, Y. Shiraishi, Y. Sugano, S. Ichikawa, S. Tanaka, T. Hirai, *ACS Catal.* **2012**, *2*, 599–603.

[15]   P. Travascio, A.J. Bennet, D.Y. Wang, D. Sen, *Chem. Biol.* **1999**, *6*, 779-787.

[16]   V. Towne, M. Will, B. Oswald, Q. Zhao, *Anal. Biochem.* **2004**, *334*, 290–296.

Entry for the Table of Contents

A binary arrangement of connected input and output hydrogel-based droplet micro-reactor modules is constructed and used to implement a UV-induced photocatalytic/peroxidation nanoparticle/DNAzyme cascade with a spatiotemporal fluorescence read-out.
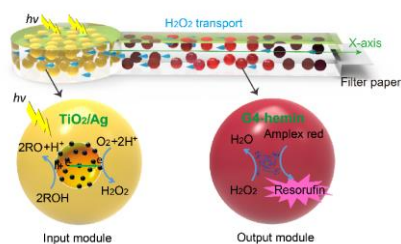
Jianbo Liu,* Liangfei Tian, Yan Qiao, Shaohong Zhou, Avinash J. Patil, Kemin Wang, Mei Li* and Stephen Mann* ***Page No. – Page No.***

Hydrogel-immobilized coacervate droplets as modular micro-reactor assemblies